Plasmon resonances in silicon nanowires: geometry effects on the trade-off between dielectric and metallic behaviour

GIOVANNI BORGH,[1,2,3] CORRADO BONGIORNO,[1] ANTONINO LA MAGNA,[1] GIOVANNI MANNINO,[1] ALIREZA SHABANI,[2] SALVATORE PATANÈ,[3] JOST ADAM,[2,4,5] AND ROSARIA A. PUGLISI[1,4,*] ●

[1]*Institute for Microelectronics and Microsystems (IMM), National Research Council (CNR), Strada Ottava 5, Zona Industriale, 95121 Catania, Italy*
[2]*Computational Materials Group, Centre for Photonics Engineering, Mads Clausen Institute (MCI), University of Southern Denmark (SDU), 5230 Odense M, Denmark*
[3]*Department of Mathematics and Computer Science, Physics and Earth Science (MIFT), University of Messina, Viale F. Stagno d'Alcontres, 31, 98166 Messina, Italy*
[4]*Contributed equally*
[5]*jostadam@sdu.dk*
[*]*rosariaanna.puglisi@cnr.it*

Abstract: Surface plasmons (SP) arising from nanometer silicon objects allow control and manipulation of light at the nanoscale exhibiting significant advantages in a plethora of applied research areas such as nanophotonic, environment, energy, biology, and medicine. These SP can achieve more significant potential, thanks to the industrial scalability and low cost offered by silicon compared with other metals and semiconductor nanosized materials. However, as they have not yet been fully understood and exploited, silicon's plasmon mechanisms need to be thoroughly studied. In particular, the influence of nanowire shape on surface plasmon behavior and the existence of physical constraints for surface plasmon excitation remains to be fully understood. In a previous study, we have demonstrated that thanks to their anisotropic one-dimensional shape, silicon nanowires sustain two types of plasmon resonances, the longitudinal ones along the main nanowire axis, with harmonic behavior and the transversal resonance, which takes place along the diameter. We demonstrated our data on a particular set of sizes, 30 nm for the diameter and about 400 nm for the length. Here we show how the resonances change when the diameter is smaller than 30 nm and the length is smaller than 400 nm. We use electron energy loss spectroscopy to map the several plasmonic modes from the fundamental one to the higher orders, with the goal of understanding how the SP resonances change when the diameter and length are smaller than 30 nm and 400 nm, respectively. We then use modeling to support the experimental findings. According to the mode order, the study illustrates the various locations inside the nanowires where discrete resonance spots can be found. Another important finding of this work is the disappearance of the surface plasmon modes for nanowires shorter than a predetermined threshold for any diameter in the range investigated, showing that the nanowire length is a key factor in maintaining electron oscillations. With this finding, a crucial physical limit for this phenomenon in silicon is established.

1. Introduction

Plasmon Resonance (PR) is a fascinating phenomenon that can be described as the coupling between an electromagnetic radiation incident on a material and the collective oscillation of electrons near the metallic-dielectric interface in that material. For the oscillation to take place, the radiation frequency has to correspond to the frequency allowed for the free electrons to oscillate.

PR is well known in the photonics and electronics community mainly because it enhances the local electrical field by concentrating electromagnetic radiation into sub-wavelength volumes [1]. This opens up a broad spectrum of applications, such as single molecule Raman detection, imaging in sub-diffraction conditions, efficient optical mixing, efficient photovoltaic conversion, enhancement of catalytic reactions and many others [2–9]. When the plasmons are excited in a system composed of a metal and a dielectric covering it, the electromagnetic waves traveling along the metal–dielectric interface are called surface plasmon polaritons (SPPs). SPPs can be excited by photons and by electrons, and involve a charge motion in the metal ("surface plasmon") and an electromagnetic wave in the dielectric ("polariton"). It is known that the resonance frequency is tunable by modulating the metallic nanostructure geometry and the characteristics of the medium surrounding it [10]. Different shapes, like nanorods or nanocubes, have been also investigated as a function of their dimension [11], demonstrating that one can tune the system plasmon features depending on the metallic nanostructure size. For these interesting scientific properties and technological applications, the literature on plasmons in metallic nanostructures is quite extensive [10,12–18]. Electron plasma oscillations have been demonstrated in semiconductor materials too, where they have been proposed to develop new exciting applications, like for example the multicolor plasmonic lasers, thermoplasmonics, biosensing, and plasma-wave Terahertz detection [19–22]. Despite the advancements in the experimental [23–26] and theoretical [27–29] fields and the huge potential in terms of industrial integration, some aspects of plasmonic resonances in silicon nanostructures are still not fully understood. In our previous work, we demonstrated that silicon nanowires (SiNWs) with a diameter of about 30 nm excited by electrons behave as an harmonic nanoresonator, showing multiple nodes/antinodes spots of the longitudinal propagating plasmon signal. By using low energy EELS (electron energy loss spectroscopy) technique, and changing the electron energy in the range 0 eV - 10 eV, we observed that the spots increase in number in correspondence of the increasing mode order [30]. The elongated shape of the silicon nanowires and their anisotropic geometry leads to a PR splitting compared to the only mode possible in highly isotropic nano-architectures, such as nanospheres [30–32]. Two resonance oscillation types are indeed allowed: the first one along the major axis, so called longitudinal, and the second one along the minor axis, the transverse resonance. The electric field related to the plasmon motion, distributes symmetrically along the major wire axis and their intensity decreases as energy increases in the range between about 4 and 6 eV [30]. This evidence indicates that SiNWs behave qualitatively in a similar way to the metallic counterparts [13]. Our previous work presented the results for a class of silicon nanowire with specific geometries. We currently do not know what happens in SiNWs with different sizes and if the plasmons exhibit dependencies on them.

In this work we present an EELS study that explores the plasmon resonances behavior in silicon nanowires when their length and diameter changes between 200 and 400 nm, and 12 and 34 nm respectively. The aim of this investigation is to understand if the geometry variation changes the discretization of the spots and if there is a size range where the resonance is not sustained. We study this behavior EELS spectral features in the energy range between 3 and 10 eV where we expect to observe the plasmonic excitations. We couple the results to simulations of the electric field spatial distribution calculated for several diameters and lengths, to explore i) the behavior in the range of sizes not covered by the experimental data, and ii) where the the silicon nanowire dielectric behavior switches to the metallic one.

2. Materials and methods

2.1. SiNWs synthesis

We carried out the silicon nanowires depositions by using a method previously demonstrated [33–35] We used silane (SiH$_4$) as a source gas and gold as the metal catalyst. The substrate used was CZ <100>13 Ω-cm p-type 6" Si wafer. After a brief HF dip, Au dots were deposited by

sputtering onto it with an equivalent thickness of Au of about 2 nm, by using a base pressure equal to 5×10^{-5} mbar, 10 mA for 60 s. The wafer was then HF dipped, dried and loaded in the CVD chamber where was heated at 380°C for 1 h before the depositions. Whereupon growth took place with the following parameters: temperature equal to 380°C, time 30 min, pressure 20 mTorr with plasma power of 20 W and a gas ratio of $SiH_4/Ar = 30$. Finally SiNWs underwent a procedure allowing the Au removal. The system was firstly dipped in a HF buffered solution diluted in H_2O (1:10) for 5 min in order to etch the SiO_2 shell; and then in a gold etch solution (Fujifilm gold etch II w/OHS) for 4 min [36]. After all the synthesis procedures, the native oxide grew on the silicon nanowires surface due to air exposure. The SiNWs were then collected from the wafer onto a metallic grid, for the TEM analysis, by mechanical stripping.

2.2. STEM analysis

The analysis was performed by STEM-EELS with JEOL ARM200 cold FEG microscope equipped with Ceos sextupole Cs aberration corrector on the probe, QuantumER Gatan imaging filter (GIF) with 0.35 eV energy resolution, dual EELS capability and advanced STEM EELS spectrum-imaging package. A spectrum image acquisition corresponds to a scan of the primary beam on a pre-selected area of the nanowire with a spatial resolution of 0.2 nm, acquiring simultaneously the high angle annular dark field signal (HAADF) and an entire EELS spectrum (0 - 0.45 eV), point by point. The result is a three-dimensional map of the single nanostructure from which it is possible to extract the EELS spectrum at any point of the nanowire or alternatively to generate a 2D image by filtering a certain energy range in the spectrum [30]. In this way it is possible to observe how a signal at a certain energy is spatially distributed. The EFSI maps were acquired only for half wire for all the SiNWs to optimize the time acquisition.

2.3. Numerical methods

We performed density-functional theory (DFT) calculations to generate the necessary high-energy optical dispersion data (Fig. S7) for bulk Si, following our previous report [30]. The calculations comprise the following specific steps. We employed the generalized gradient approximation (GGA) in the PBE form [37] to the exchange-correlation functional, optimizing the crystal structure of bulk Si by considering a double-zeta plus polarization (DZP) orbital basis set. We performed the integration in the first Brillouin zone upon a Monkhorst-Pack [38] grid of 7x7x7, along with a mesh cutoff of 300 Ry. Following experimental reports [39], we arranged the silicon atoms in form of a diamond crystal structure with space group Fd3m[227] and a lattice constant of a=5.43Å. We relaxed both lattice constant and atomic position, until the maximum force on every atom and a convergence threshold for self-consistent iterations fell below 0.02 eV/Å and 1×10^{-3} eV, respectively.

We performed finite-element method (FEM) simulations to model the optical response of isolated silicon nanowires. We employed the wave optics module of the commercially available FEM solver COMSOL Multiphysics [40]. We modeled the experimentally investigated NWs by a Si cylindrical core of varying diameter and length, surrounded 2 nm thick silicon dioxide (SiO_2) shell. We assumed slightly rounded tips to avoid exaggerated edge effects at the tips. The NW was embedded in a spherical vacuum domain, surrounded by perfectly matched layer (PML) boundaries to mimic an infinite outer domain. We excited the structure with a background electromagnetic plane wave (wavelengths between 110 and 550 nm, corresponding to energies between 11.27 eV and 2.25 eV, respectively), with an electrical field amplitude of $1 \, V \, m^{-1}$, impinging perpendicularly to the NW longitudinal axis and polarized both in parallel and orthogonal to the long NW axis. We modeled the crucial Si and SiO_2 material influence on the optical simulations via complex-valued, dispersive refractive index data. The SiO_2 data set is based on literature values [41].

3.   Results and discussion

We selected the SiNWs by dimension and characterized them by EELS and STEM. Figure 1 reports the energy-filtered spectroscopic images (EFSI) acquired for a typical silicon nanowire from the group with an average Si diameter of about 30 nm and length of about 300 nm. Specifically the SiNW imaged presents a diameter of 34 nm, length equal to 314 nm, and a SiO_2 shell 1.4 nm thick. The Figure reports the energy-filtered spectroscopic images (EFSI) maps at different energies: 3.9 eV, 4.5 eV, 5.3 eV, 6.5 eV and 8.5 eV, chosen in correspondence of the maximum intensity of the signals. We can note that a very intense signal spot is localized on the wire tip and this is attributed to the tip effect [42]. As described in the Materials and methods Section, the EFSI maps were acquired only for half wire for all the silicon nanowires to optimize the acquisition time.
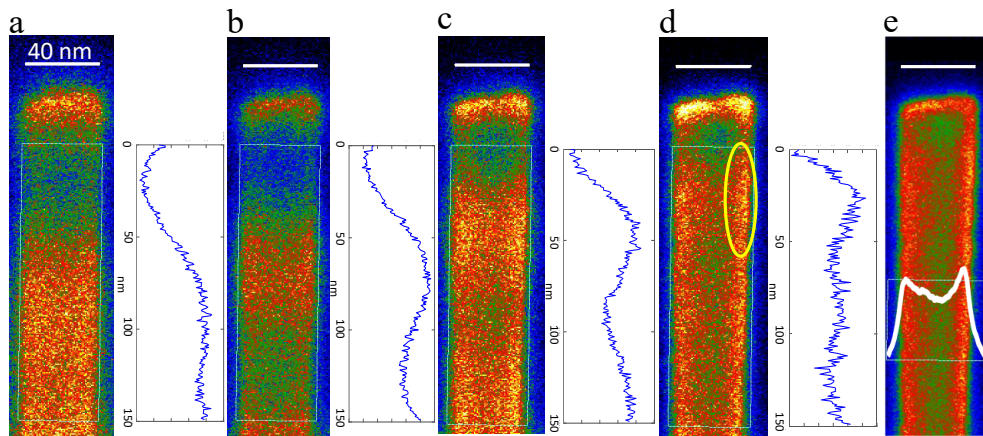

Fig. 1. EFSI maps acquired at five different energies for a NW with Si diameter equal to 34 nm and length of 314 nm taken at: 3.9 eV, 4.5 eV, 5.3 eV, 6.5 eV and 8.5 eV. The resonance at 8.5 eV corresponds to the transverse PR. Axially extracted EELS signal profiles are reported on the right of each map

Figure 1(a) corresponds to the map at 3.9 eV. It shows an extended area with a signal spot distributed symmetrically along the major wire axis. The blue curve, reported in the graph on the right shows the corresponding peak. It is likely due to the tail of a scattering signal, allowed at this energy as explained below.

Figure 1(b) shows the 4.5 eV map exhibiting a spot and a half along the axis. For symmetry reasons, at this energy, a total of three spots are present on the entire wire. We also note that the top lobe is now closer to the tip. The relative signal intensity profile on the right (blue curve) displays this behavior. At 5.3 eV (Fig. 1(c)) we observe the same trend as in Fig. 1(b) but more pronounced, i.e. the presence of the one and a half lobes corresponding to the spot of the first harmonic and to the scattering signal seen at 3.9 eV still present. At this energy the harmonic is excited more sharply and it is more distinguishable than at 4.5 eV. In Fig. 1(d) at 6.5 eV it is possible to observe the successive harmonic with two and a half spots, with a total of five spots present in the NW entire structure. This resonance presents a less intense signal than the previous ones, as expected. It is indeed known that the intensity decreases as the order increases. Moreover, we can observe, as expected in harmonic oscillators, that the energy difference between two successive plasmon modes reduces as the energy is swept to larger values. The signal patterns above described can be interpreted as the result of the interference of propagating SPPs in which the spots represent the nodes, while the low intensity areas correspond to the antinodes. The SPPs propagate back and forth along the nanowire major axis and are reflected at the edges of the

tip, giving rise to the interference fringes similar to a standing wave. As the energy increases, the number of nodes increases. The result is a behavior similar to that of a nano-oscillator that can sustain higher order harmonics.

The map in the Fig. 1(e) extracted at 8.5 eV, at a well separated energy with respect to the longitudinal modes, shows instead the plasmon resonance signal with transversal nature. This plasmonic signal is located at the interface between Si and SiO_2 as shown by the intensity profile (white curve) in the inset.

For this group of investigated SiNWs we can conclude that the harmonic behavior of the longitudinal and transversal resonances follow the resonator behavior.

Figure 2 reports the EFSI maps for half silicon nanowire from a group of nanostructures with an average diameter of about 20 nm and lengths of about 400 nm. Specifically the SiNW imaged has a core diameter of 26 nm and length of 411 nm. The figure reports the TEM results at the energies where the most significant signals appear: 3.9 eV, 4.5 eV, 5.3 eV, 6.5 eV and 8.5 eV.
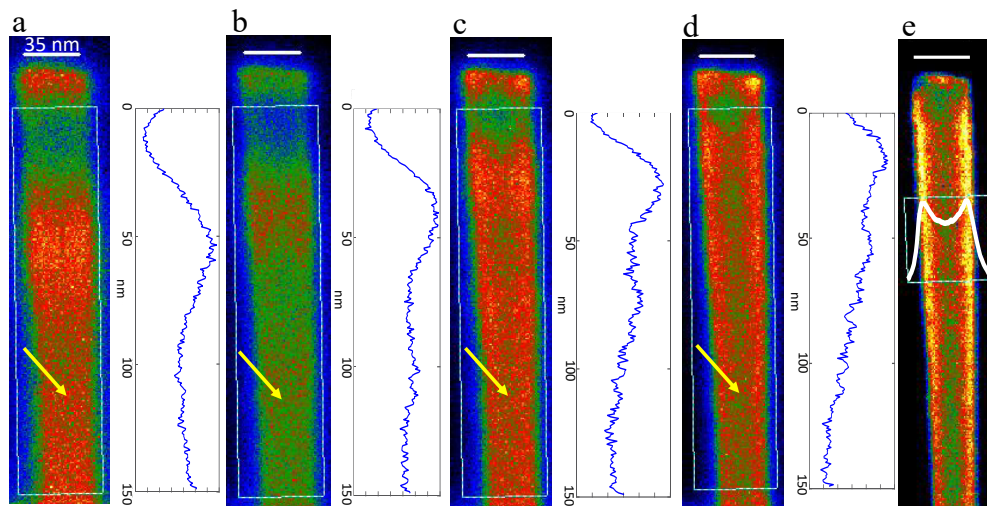

Fig. 2. EFSI maps acquired at five different energies for NW with Si core diameter equal to 26.25 nm and length of 411 nm depicts the harmonics at: 3.9 eV, 4.5 eV, 5.3 eV, 6.5 eV. The resonance at 8.5 eV corresponds to the transverse plasmon resonance. White rectangles indicate the areas from which the EELS signal profiles, reported on the right of each map, are axially extracted

As it is possible to observe, at 3.9 eV we find two separate spots. They represent the sum of two contributions, the fundamental longitudinal harmonics and a contribution which we attribute to a scattering phenomenon. We will discuss better this aspect later. In the EFSI maps taken at 4.3, 5.3 and 6.5 eV reported in Fig. 2(b-d) and their relative intensity profiles on the right (blue curves) we find the same situation seen in Fig. 1. Thus we confirm that the harmonic spots increase in number with increasing energy also when the silicon nanowires have this dimension. In Fig. 2(e), at about 8.5 eV, it is again observed the transverse plasmonic peak, localized at the interface between the semiconductor and oxide shell (white curve, inset, representing the intensity profile).

Figure 3 shows the EFSI maps of the spatial distribution of the electric field processed for a silicon nanowire group with an average diameter of about 10 nm and length of roughly 200 nm. More precisely, the SiNW reported here presents a core diameter of 12.5 nm and 189 nm of length. Differently from the previous case, here with half of the diameter and length size, an approximately uniform distribution along the major wire axis is observed and no discrete spots

are present, except for the 5.3 eV case, where we note two peaks in the signal profile reported on the right, although not well defined. The disappearance of the harmonic behavior can be attributed to the reduced length of the wires with respect to the previous ones shown in Fig. 1 and Fig. 2. A possible explanation is that the intensity spots are so close that they overlap spatially and are not clearly distinguishable as in the previous cases. From these data we understand that the resonator length is an important parameter to observe the longitudinal modes, although the simulations are needed to further deepen these preliminary understandings. A general trait of all the experimental observations shown so far, is that the spots in this nano-sized semiconductor material, are more spatially and energetically diffused with respect to the signals typical of metallic resonators, in accordance to what already reported [30].
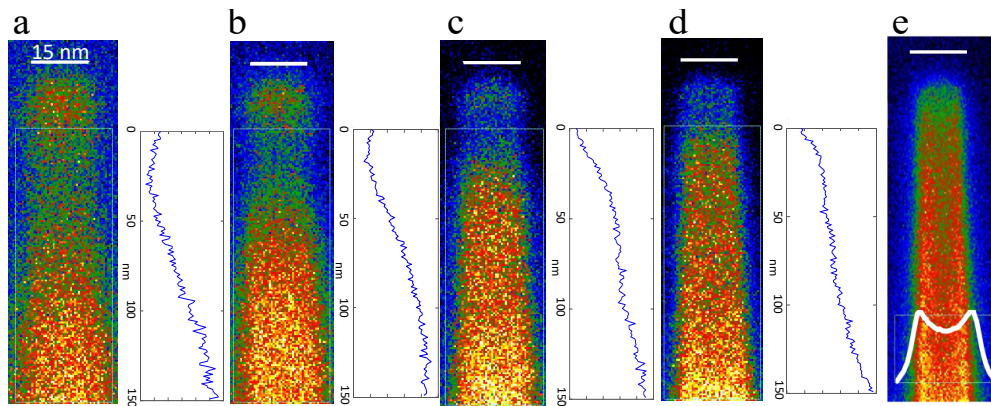

Fig. 3. EFSI maps for SiNW with core diameter equal to 12.75 nm and length of 189 nm at five different energies: 3.9 eV, 4.5 eV, 5.3 eV, 6.5 eV. The resonance at 8.5 eV corresponds to the transverse plasmonic resonance. White rectangles indicate the areas from which the EELS signal profiles, spectra on the right of each map, are axially extracted.

3.1. Numerical results and comparison with the experimental characterization

To fully explain the physics behind our experimental observations, we then calculated the optical absorption and scattering cross-sections (Fig. 4), and corresponding electromagnetic (EM) near-field patterns (Fig. 5), exemplary for the NW with the class size of 26 nm diameter and 411 nm length, the (26,411) case. The choice to start with this family of silicon nanowires is due to the fact that the (34, 314) case reported in Fig. 1 is similar in the diameter dimension to what we have already simulated in our former paper [30], i.e. (30, 420) and as stated above we are now interested in investigating also the role of the NWs length.

Figure 4 reports optical dispersion data for the (26,411) case, for longitudinal (solid lines) and transversal (dashed lines) incident light polarization, where the incident electric field is parallel or normal to the main NW axis, respectively. As the curves indicate, in the case of the longitudinal polarization, the NW starts absorbing the EM field at energies larger than 2.47 eV. The absorption increases until 2.8 eV, where it exhibits a plateau. A further increase in energy produces a sharp peak at around 4.0 eV, which corresponds to one of the prominent plasmon peaks in the silicon nanowire. It is interesting to note that for energy values higher than 4.1 eV, several tiny peaks appear indicating the higher-order resonances. The scattering curve approximately follows the absorption for all the energy spectrum, except for a strong peak at 2.58 eV, suggesting an interaction between the incident light and the SiNW. In transverse polarization, dashed curves, there is one significant excitation resonance at the energy of 10.33 eV. Here the electromagnetic field interaction with the NW results in a higher scattering rate i) than the absorption in the same
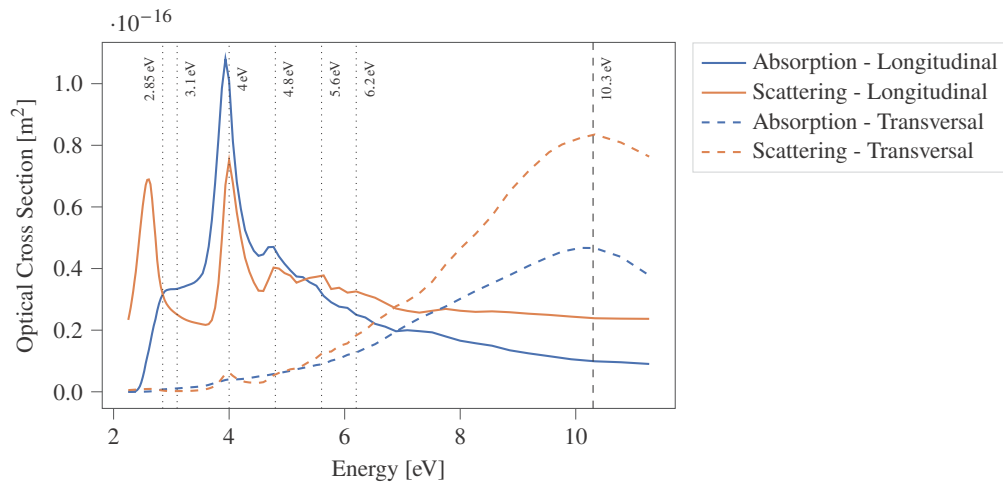
Fig. 4. Absorption and scattering cross sections for the (26,411) nanowire. Solid lines: longitudinal polarization, dashed lines: transverse polarization (with respect to the NW's long axis). The vertical lines mark the plasmonic resonances, as visualized in Fig. 5, corresponding to the major peaks in the absorption spectrum.

energy range, and ii) with respect to the low energy range, where it interacts with the Si bulk material primarily through absorption.

It is worth noting that the simulated spectrum exhibits broad and distinct peaks at high energies for transverse polarization, and in the other regime the peaks disappeared, witnessing the change of regime from the longitudinal to the transverse resonance observed experimentally. This will be also further discussed later.

To visualize the scattering and dissipation phenomena, in Fig. 5 we report the electric field (EF) and electromagnetic power loss density (PL) pattern relative to the same silicon nanowires class size. The latter describes the dissipation of the incident beam's energy through the heating process originating from the oscillating electrons absorbing the EM beam.

We have calculated the optical cross-section plots in correspondence with the most peculiar energy values found during the experimental investigations, i.e. from 2.25 eV to 10.3 eV. Figure 5 reports the electric field norm (EF), first image, and power loss (PL), successive images. The separate plots show different scales, each normalized to the minimum and maximum EF/PL values taken inside the individual simulation volume. The first image, corresponding to the EF pattern, presents a range of intensity extending from 0.24 to 4.12 V m^{-1}. A value ranging between 1.5 and 2 V m^{-1} is found at the NW center, while the highest value in correspondence of a very confined region at the NW tips. For high energy values, we calculated the electromagnetic PL plots, as one expects to see the starting point for the absorption edge at about 2.47 eV. A region with low-rate absorption inside the NW is seen at 2.25 eV. By increasing the energy, the absorption rate at 2.85 eV is more significant than at 2.25 eV, reaching plateau values in the order of 1×10^5 for the absorption spectrum between 2.85 eV and 3.1 eV. We address the origin of this phenomenon to the inter-band transition peak at the energy of 2 eV in the dielectric permittivity's imaginary part, reported in the Supplement 1 file, showing the process of absorption and re-emission of EM waves by the electrons in the atomic orbitals. The results show the presence of the electric field almost completely inside Si, suggesting that it is a semiconducting behavior for the nanostructure. By further increasing the energy, this "hot" region gradually fades, as different light-matter mechanisms appear. At 3 eV we can see that the hot region slightly moves outward, and two lobes appear in the opposite NW side, on the left of the structure. We interpret this shift as
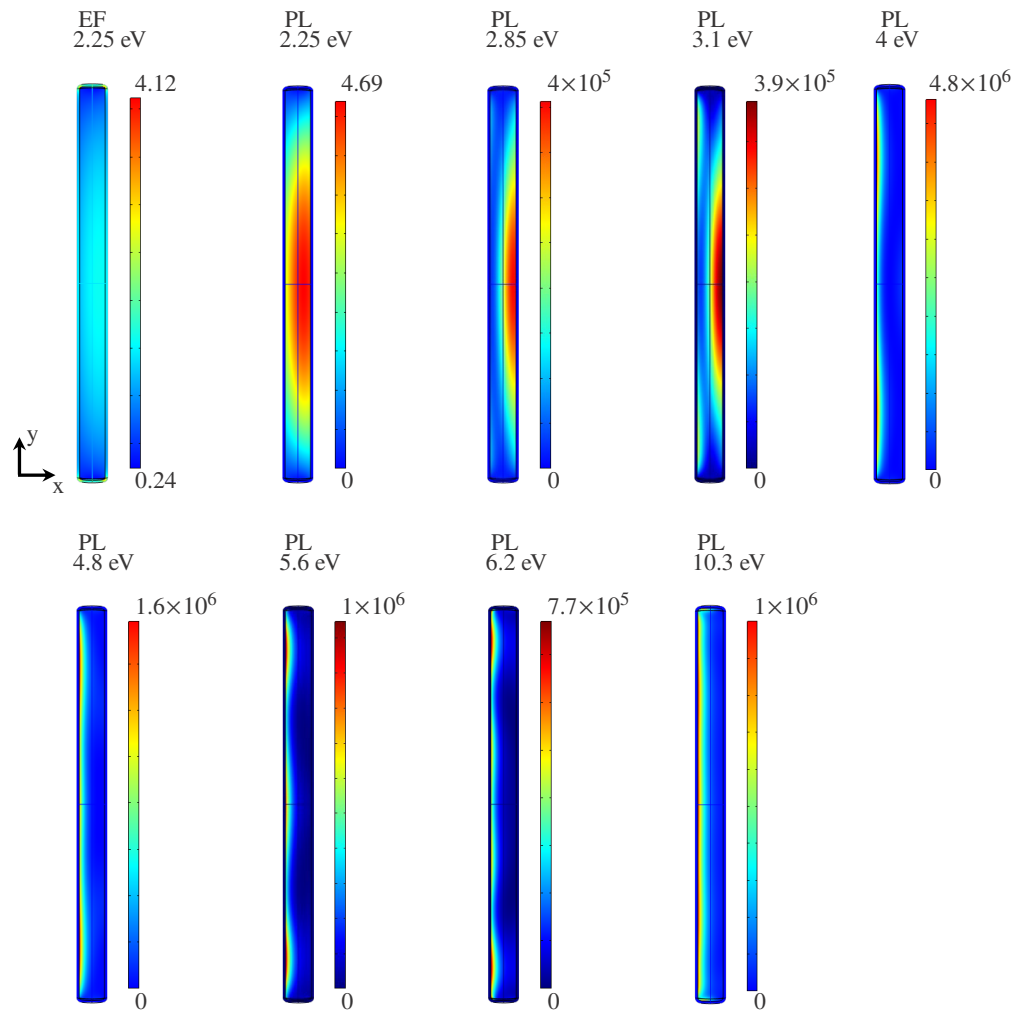
Fig. 5. Electric field norm (EF) [$V\,m^{-1}$] and power loss (PL) [$W\,m^{-3}$] on the (26,411) nanowire.

a gradual shift, with increasing energy, from semiconducting to metallic behavior. The PL pattern at the wavelength of 4 eV demonstrates two hot spots, indicating the first order of surface plasmon resonance at the Si-SiO$_2$ interface. At this energy, the local field enhancement and the PL density peaks only appear at the interface. First, the evanescent electric fields result purely from oscillating electrons at the NW-shell interface (plasmons). Secondly, the evanescent fields are not permitted further inside the silicon domain, confirming silicon's metallic characteristics at higher energies; the EM fields only penetrate a few nanometers, according to the penetration depth. We also have the highest value for the PL intensity among the respective plots for different wavelengths in the longitudinal polarization (shown in the respective legend), matching well with the highest peak in the absorption spectrum of the (26,411). By further increasing the energy, the next excitation resonance gradually appears. The third hot spot starts showing up exactly at the NW center, at the energy of 4.8 eV. It is a mixture of first and second modes showing two and three lobes, respectively. The second mode is excited more sharply at 5.6 eV, where it is clearly distinguishable. A further energy increase shows the excitation of a third-order surface plasmon

resonance in the NW with four lobes along the main axis, at 6.2 eV. It is worth noting that the energy difference between two successive plasmon modes shrinks as the energy is swept to higher values and with increasing the resonance order, as expected from theory and as observed experimentally.

For the transverse polarization, we have simulated the irradiation of the NW by an harmonic electromagnetic beam propagating along the *x*-direction with an electric field along the *z*-direction. The prominent peak (absorption/scattering) occurs at the energy of 10.33 eV, as illustrated in the plasmonic pattern of the Figure. It appears as an intense spot all along the NW length, only on wall of the nanostructure, originating from a pronounced localized plasmon excitation.

From all the above considerations on the calculated patterns, it is evident that the PL density reproduces very well the phenomena that we experimentally observed by EELS and they take place at the interface between silicon and SiO_2. It can as well be concluded that the PL density representation is the correct tool for the proper recognition of the plasmon resonances, since the electric field patterns tend to overexpose the contributions of the hot spots at the tips and the sharp edges of the structure, covering the low-intensity lobes of the plasmon resonances in the center of the SiNWs and eventually leading to a non-accurate recognition of the PR modes. It is worth noting that the simulations results replicate well the experimental data. The slight mismatch between the simulated resonance energies and the experimental findings, is attributed to the following reasons: i) the DFT-calculated Si data refers to bulk Si and neglect geometry and lattice related confinement effects; ii) the SiO_2 shell stoichiometry and morphology could further influence the resonance positions.

The main purpose of this paper is to understand the plasmon resonance behavior when the silicon nanowires change sizes and to establish which is the size limit within which they can support the excitation. To investigate the impact of the SiNW dimension on the plasmon resonances and to address the behaviour of the expected resonances in the range of sizes not covered by the experimental observation, we have considered four different values of diameters and lengths. Despite the fact that our experimental measurements are not limited to the two cases (12,189) and (26,411), we consider these cases as the verification basis for our simulations because more representative of the physical phenomena taking place, and extend numerically to more cases by changing in diameter and length based on their combination. To this end, in the simulation part, we investigate the optical properties of two more NWs, altering the NW dimensions, resulting in (the purely numeric) (12,411) and (26,189) cases (see Figs. S1-S6 for numerical cross-section and near-field analyses). We thereby study the dimension effect for a set of four different SiNWs varying in diameter and length, as the rectangle corners shown in Fig. 6.

To validate our model, we first compare the PL profiles for plasmon modes of the (26,411) NW with PL measurements in Fig. 1. For the simulations (See Fig. 5), the first plasmon mode is excited at the energy of 4 eV, while the PL measured shows the first mode at 3.9 eV. In this mode, one complete lobe is excited in the half-length of NW in measurement, while the simulations show the same behavior as there are two hot spots through the whole length of NW. Measurements indicate that the second mode is excited at the energy of 4.5 eV with one full lobe plus half of the lobe in half-length of NW. The simulation matches well in the PL profile as it contains three hot spots through the whole NW length, except this mode starts to be excited at the energy of 4.8 eV and extends to 5.6 eV. The next mode occurs at the energy interval of 5.3 eV to 6.5 eV for measurements, containing two distinct hot spots over the half-length of NW. The simulations show the same behavior as there are four lobes along the whole length of NW at the energy of 6.2 eV, as two lobes with high intensity close to the NW tips against two other lobes with low intensity around the NW center. For the transverse polarization, there is one pronounced plasmon mode for both measurements and simulations, whereas they occur at different energies of 8.5 eV and 10.3 eV, respectively.
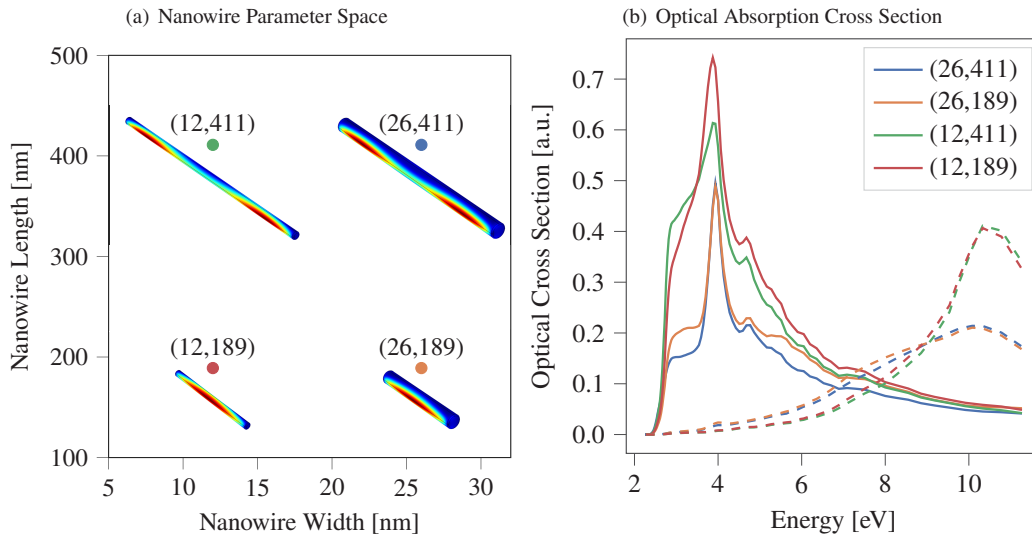
Fig. 6. (a) Nanowire parameter space for 4 numeric cases: (12,411), (26,411), (12,189), (26,189). (b) Optical absorption cross section for the same 4 rectangle corners as in (a), reporting the longitudinal polarization (solid lines) and the transverse polarization, with respect to the NW's long axis (dashed lines).

Comparing the simulated (12,189) NW results (Figs. S5 and S6) with the experimental measurements, one can see that the overall shape of the optical cross-sections, including absorption and scattering, does not change upon geometry alteration in the simulations. The same was observed in experimental measurements, as the excited plasmon energies do not change if we compare (12,189) with (26,411) cases. The first spot, centralized in the NW middle, is observed at the energy of 3.9 eV. The measurement shows the same behavior, as half of the lobe appears in the half-length of NW at the energy of 3.9 eV. By increasing energy, one can see that together with this lobe two separated lobes gradually appear in each NW's half-length indicating the first resonance. The successive mode appears at the energy interval of 5.3 eV to 6.5 eV for the experiment, including two separate lobes over the NW half-length, one in the NW center and another extended toward the NW tip. The simulations represent three hot spots along the whole length of NW at the energy of 6.2 eV. Like the (26,411) case, in the transverse polarization, there is one pronounced plasmon mode for both measurements and simulations, again occurring at different energies of 8.5 eV and 10.3 eV, respectively. From these observations we can understand that the plasmonic resonances all present the same trend in the transversal excitation, regardless the silicon nanowire size. The major differences are noted in how the scattering switches to absorption and vice versa, because the large NWs exhibit mainly scattering, while the thin ones have larger absorption. The simulations then support the experimental findings and cover the missing information where the data are not present. The results obtained here show that the plasmon resonances can get excited in silicon nanowires, that the phenomenon is observable for a certain length range, down to a threshold above which the structure does not sustain the oscillations anymore. This is an important result because defines the limits for the plasmons to get excited in such small architectures. These findings open however new questions to be answered in the future, among the others: the role of the lattice related confinement, the shell stoichiometry and morphology, and other fine aspects related to the length of the structures and the high order modes in the transversal resonances.

4. Conclusion

In this work the geometry variations effect on the low energy EELS plasmonic features for silicon nanowires has been studied. We investigated several diameters and lengths in the ranges of about $10 - 30$ nm and $200 - 400$ nm, respectively. The results confirm that the SiNWs support two types of SPRs: the longitudinal and the transverse ones. The longitudinal modes have a harmonic behaviour and their spots intensity distributes symmetrically along the major axis of the silicon nanowires, increasing in number as energy increases. The transversal mode gets excited at high energies, separated from the longitudinal ones and it is located along the wall of the nanostructures, and at the interface between Si and SiO_2. We have observed that by reducing the wire length to $10 - 189$ nm, the longitudinal harmonic spots become indistinguishable between each other. Our direct observations allowed us to demonstrate that, when scanning over the energy, the scattering spots gradually give space to the longitudinal plasmonic resonances, marking the transition from the semiconducting to the metallic behavior of our nanostructures. Besides the energy, also the SiNW dimension plays a role: the scattering switches to absorption and vice versa depending on the diameter, with the large NWs exhibiting mainly scattering, while the thin ones predominantly the absorption. The transversal PR excitation does not show appreciable changes with the silicon nanowires dimension. This is the first time to the best of our knowledge that these data are shown. Understanding plasmonic resonances in silicon nanoparticles in the dimensional regime where the structure's size is well below the diffraction limit at the plasmon wavelengths, establishes the frame in which these phenomena can be observed and how they might be practically used.

Disclosures. The authors declare no conflicts of interest.

Data availability. No data were generated or analyzed in the presented research.

Supplemental document. See Supplement 1 for supporting content.

References

1. S. Maier, *Plasmonics: Fundamentals and Applications* (Springer, 2007).
2. S. Nie and S. R. Emory, "Probing single molecules and single nanoparticles by surface-enhanced Raman scattering," Science **275**(5303), 1102–1106 (1997).
3. K. Bosnick, Jiang, and B.L. , "Fluctuations and local symmetry in single-molecule rhodamine 6G Raman scattering on silver nanocrystal aggregates," J. Phys. Chem. B **106**(33), 8096–8099 (2002).
4. J. B. Pendry, "Negative refraction makes a perfect lens," Phys. Rev. Lett. **85**(18), 3966–3969 (2000).
5. P. Anger, P. Bharadwaj, and L. Novotny, "Enhancement and quenching of single-molecule fluorescence," Phys. Rev. Lett. **96**(11), 113002 (2006).
6. P. Mühlschlegel, H.-J. Eisler, O. J. F. Martin, B. Hecht, and D. W. Pohl, "Resonant optical antennas," Science **308**(5728), 1607–1609 (2005).
7. E. J. Sánchez, L. Novotny, and X. S. Xie, "Near-field fluorescence microscopy based on two-photon excitation with metal tips," Phys. Rev. Lett. **82**(20), 4014–4017 (1999).
8. H. A. Atwater and A. Polman, "Plasmonics for improved photovoltaic devices," Nat. Mater. **9**, 215–219 (2010).
9. P. Camargo and E. Cortés, "Plasmonic catalysis," *From Fundamentals to Applications*, pp. 1–352 (Wiley, 2021).
10. Y. Wu, G. Li, and J. P. Camden, "Probing nanoparticle plasmons with electron energy loss spectroscopy," Chem. Rev. **118**(6), 2994–3031 (2018).
11. Y.-Y. Cai, S. S. E. Collins, M. J. Gallagher, U. Bhattacharjee, R. Zhang, T. H. Chow, A. Ahmadivand, B. Ostovar, A. Al-Zubeidi, J. Wang, P. Nordlander, C. F. Landes, and S. Link, "Single-particle emission spectroscopy resolves d-hole relaxation in copper nanocubes," ACS Energy Lett. **4**(10), 2458–2465 (2019).
12. I. Alber, W. Sigle, S. Müller, R. Neumann, O. Picht, M. Rauber, P. A. Van Aken, and M. E. Toimil-Molares, "Visualization of multipolar longitudinal and transversal surface plasmon modes in nanowire dimers," ACS Nano **5**(12), 9845–9853 (2011).
13. D. Rossouw, M. Couillard, J. Vickery, E. Kumacheva, and G. A. Botton, "Multipolar plasmonic resonances in silver nanowire antennas imaged with a subnanometer electron probe," Nano Lett. **11**(4), 1499–1504 (2011).
14. A. Losquin and M. Kociak, "Link between cathodoluminescence and electron energy loss spectroscopy and the radiative and full electromagnetic local density of states," ACS Photonics **2**(11), 1619–1627 (2015).

15. R. Qi, R. Wang, Y. Li, Y. Sun, S. Chen, B. Han, N. Li, Q. Zhang, X. Liu, D. Yu, and P. Gao, "Probing far-infrared surface phonon polaritons in semiconductor nanostructures at nanoscale," Nano Lett. **19**(8), 5070–5076 (2019).

16. J. Niedziółka-Jönsson and S. Mackowski, "Plasmonics with metallic nanowires," Materials **12**(9), 1418 (2019).

17. G. Zheng, S. Mourdikoudis, and Z. Zhang, "Plasmonic metallic heteromeric nanostructures," Small **16**(38), 2002588 (2020).

18. Z. Gu, Q. Song, and S. Xiao, "Nanowire waveguides and lasers: advances and opportunities in photonic circuits," Front. Chem. **8**, 613504 (2021).

19. J. A. Sánchez-Gil and J. G. Rivas, "Thermal switching of the scattering coefficients of terahertz surface plasmon polaritons impinging on a finite array of subwavelength grooves on semiconductor surfaces," Phys. Rev. B **73**(20), 205410 (2006).

20. C. Li, Z. Liu, J. Chen, Y. Gao, M. Li, and Q. Zhang, "Semiconductor nanowire plasmonic lasers," Nanophotonics **8**(12), 2091–2110 (2019).

21. B. Yao, Z. B. Fang, Y. Y. Zhu, T. Ji, and G. He, "A model for the frequency dispersion of the high-k metal-oxide-semiconductor capacitance in accumulation," Appl. Phys. Lett. **100**(22), 222903 (2012).

22. A. Agarwal, M. S. Vitiello, L. Viti, A. Cupolillo, and A. Politano, "Plasmonics with two-dimensional semiconductors: from basic research to technological applications," Nanoscale **10**(19), 8938–8946 (2018).

23. V. Kashyap, N. Chaudhary, N. Goyal, and K. Saxena, "Fabrication and characterization of silicon nanowires with MACE method to influence the optical properties," Mater. Today: Proc. **49**(1), 3409–3413 (2022).

24. S. Ahoulou, E. Perret, and J. Nedelec, "Functionalization and characterization of silicon nanowires for sensing applications: a review," Nanomaterials **11**(4), 999 (2021).

25. W. Liu, Y. Wang, X. Guo, J. Song, X. Wang, and Y. Yi, "Light trapping in single elliptical silicon nanowires," Nanomaterials **10**(11), 2121 (2020).

26. B. S. Swain, B. P. Swain, and N. M. Hwang, "Investigation of electronic configuration and plasmon loss spectra in Au-catalyzed silicon nanowire networks," J. Appl. Phys. **108**(7), 073709 (2010).

27. S. Ossicini, I. Marri, M. Amato, M. Palummo, E. Canadell, and R. Rurali, "Ab initio studies of the optoelectronic structure of undoped and doped silicon nanocrystals and nanowires: the role of size, passivation, symmetry and phase," Faraday Discuss. **222**, 217–239 (2020).

28. Y. Yang, Z. Lu, D. Liu, Y. Wang, S. Chen, and T. Li, "A theoretical and simulation analysis of the sensitivity of SiNWs-FET sensors," Biosensors **11**(4), 121 (2021).

29. X. R. Zhuo and H. G. Beom, "Effect of side surface orientation on the mechanical properties of silicon nanowires: a molecular dynamics study," Crystals **9**(2), 102 (2019).

30. G. Borgh, C. Bongiorno, A. La Magna, G. Mannino, S. Patanè, J. Adam, and R. A. Puglisi, "Surface plasmons in silicon nanowires," Adv. Photonics Res. **2**(12), 2100130 (2021).

31. J. Wang, X.-J. Wang, Y. Jiao, M.-W. Chu, M. Malac, and Q. Li, "Surface plasmon resonance in interacting si nanoparticle chains," Nanoscale **2**(5), 681–684 (2010).

32. Z. R. Lawson, A. S. Preston, M. T. Korsa, N. L. Dominique, W. J. Tuff, E. Sutter, J. P. Camden, J. Adam, R. A. Hughes, and S. Neretina, "Plasmonic gold trimers and dimers with air-filled nanogaps," ACS Appl. Mater. Interfaces **14**(24), 28186–28198 (2022).

33. R. A. Puglisi, C. Bongiorno, S. Caccamo, E. Fazio, G. Mannino, F. Neri, S. Scalese, D. Spucches, and A. La Magna, "Chemical vapor deposition growth of silicon nanowires with diameter smaller than 5 nm," ACS Omega **4**(19), 17967–17971 (2019).

34. C. Garozzo, A. La Magna, G. Mannino, V. Privitera, S. Scalese, P. M. Sberna, F. Simone, and R. A. Puglisi, "Competition between uncatalyzed and catalyzed growth during the plasma synthesis of Si nanowires and its role on their optical properties," J. Appl. Phys. **113**(21), 214313 (2013).

35. R. A. Puglisi, G. Mannino, S. Scalese, A. L. Magna, and V. Privitera, "Silicon nanowires obtained by low temperature plasma-based chemical vapor deposition," MRS Proc. **1408**, 139–144 (2012).

36. R. A. Puglisi, C. Bongiorno, G. Borgh, E. Fazio, C. Garozzo, G. Mannino, F. Neri, G. Pellegrino, S. Scalese, and A. La Magna, "Study on the physico-chemical properties of the Si nanowires surface," Nanomaterials **9**(6), 818 (2019).

37. J. P. Perdew, K. Burke, and M. Ernzerhof, "Generalized gradient approximation made simple," Phys. Rev. Lett. **77**(18), 3865–3868 (1996).

38. H. J. Monkhorst and J. D. Pack, "Special points for Brillouin-zone integrations," Phys. Rev. B **13**(12), 5188–5192 (1976).

39. J. Zemann, "Crystal structures," Acta Crystallogr. **18**(1), 139 (1965).

40. COMSOL - Software for Multiphysics Simulation

41. L. Gao, F. Lemarchand, and M. Lequime, "Refractive index determination of Si_2 layer in the UV/Vis/NIR range: spectrophotometric reverse engineering on single and bi-layer designs," J. Eur. Opt. Soc. **8**, 13010 (2013).

42. J. Grand, M. L. de la Chapelle, J.-L. Bijeon, P.-M. Adam, A. Vial, and P. Royer, "Role of localized surface plasmons in surface-enhanced raman scattering of shape-controlled metallic particles in regular arrays," Phys. Rev. B **72**(3), 033407 (2005).